

Singularity Avoidance for Over-Actuated, Pseudo-Omnidirectional, Wheeled Mobile Robots

Christian P. Connette, Christopher Parltz, Martin Hägele, Alexander Verl

Abstract—For mobile platforms with steerable standard wheels it is necessary to precisely coordinate rotation and steering angle of their wheels. An established approach to ensure this is to represent the current state of motion in form of the Instantaneous Centre of Motion (ICM) and to derive a trajectory within this space. However, while control in the ICM space does guarantee adherence to the system’s non-holonomic constraints, it does not avoid the system’s singular configurations. Within this work we address the problem of singularity avoidance within the ICM space. Singularities related to the mathematical representation of the ICM are reduced by a reformulation of this representation. Furthermore, a controller based on artificial potential fields avoiding singular configurations of the robot by representing them as obstacles in the derived ICM space is designed. The resulting controller is particularized and analyzed w.r.t. the Care-O-bot 3 demonstrator.

I. INTRODUCTION

Mobile service robots operating in domestic environments, need a high degree of flexibility and agility [1]. Thus, over the last decades a wide variety of different motion concepts [2] was investigated. Currently, wheeled platforms appear to be a promising compromise between a high degree of flexibility, robustness and moderate complexity. The approaches in this field range from differential driven platforms and systems with centered or off-centered orientable wheels to mobile robots that use specially designed wheels [3], [4]. To balance such requirements against design matters such as a small footprint and size of the overall system, the mobile base of the service robot platform Care-O-bot 3 (Fig. 1) was composed by four orientable standard wheels.

According to the work by Campion, Bastin and D’Andréa-Novel [5], such a robot has 3 degrees of freedom (DOF) and these DOFs split into the degree of steerability $\delta_s = 2$, associated to the number of independable steerable wheels, and the degree of mobility $\delta_m = 1$, associated to the instantaneously accessible velocity space for the planar motion. Thus, Care-O-bot 3 is a pseudo-omnidirectional mobile robot able to realize arbitrary velocity and rotational commands, however only after reorienting its wheels. Furthermore, this means that all wheels have to be precisely coordinated to ensure adherence to the system’s non-holonomic constraints.

Besides a variety of different approaches [6], [7], [8], an often applied strategy to this problem is to control the robot via its Instantaneous Centre of Motion (ICM) [9], [10], [11]. However, the ICM-based representation has in



Fig. 1. Mobile base of Care-O-bot 3, without coating (www.care-o-bot.de)

its standard formulation some numerical drawbacks, which affect potential control strategies [12]. Also, while control of the ICM guarantees compliance to the robots nonholonomic constraints, it does not account for the system’s singularities. For instance, the control scheme proposed in [12] solves this problem by constraining the accessible velocity space of the robot to a region without singular configurations. This need for the avoidance of singular regions is analogous to the problem of obstacle avoidance for mobile robots. Potential fields [14], [15] have been successfully applied to such global and local path planning problems [16] and most effective to local obstacle avoidance problems [17]. Shimoda et. al. [18] even applied potential fields not only to represent obstacles but also to express system dynamics in the “trajectory space”.

Within this work, we address the topic of singularities related to control of the robot motion via the ICM. We classify the arising singularities into those resulting from the mathematical representation of the ICM [13] and those resulting directly from the system’s kinematics. We shortly review a method which remedies problems resulting from the singularities mentioned first by rewriting the ICM as a spherical coordinate representation of the robots twist $\vec{t} = (v_x, v_y, \omega)^T$. To approach problems arising from the second type of singularities we propose the usage of a potential field based controller. We illustrate how singularities in the robot’s configuration can be expressed as repulsive potentials in the proposed ICM space. Finally, we particularize the derived controller with respect to the Care-O-bot 3 demonstrator (Fig. 1) and analyze it simulative and experimental. At first however, we give an overview on our system architecture and the resulting implications for our controller.

This work was conducted in the department for Robotic Systems at the Fraunhofer Institute for Manufacturing Engineering and Automation (IPA), 70504 Stuttgart, Germany; Contact: christian.connette@ipa.fraunhofer.de

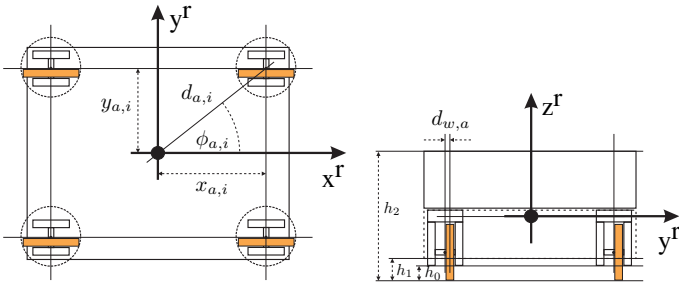


Fig. 2. Top and front view of Care-O-bot 3's mobile base

II. SYSTEM OVERVIEW

The platform (Fig. 1 and Fig. 2) has an rectangular shape with a length of approximately 60 cm and a width of about 50 cm. The steering-axes of the wheels lie at $x_{a,i} = \pm 23,5$ cm and $y_{a,i} = \pm 18,5$ cm. The wheels are sideways off-centered to the steering-axes by $d_{w,a} = 2,2$ cm. The chassis clearance h_1 is about 5 cm. The total height of the system h_2 is approximately 35 cm.

The control-software of the mobile platform has a multi-layer structure. Current and velocity control for the actuators is provided by off-the-shelf motor controllers. The lowest software-layer comprises the control loop for the robot velocities (v_x, v_y, ω) generating the set point values $(\vec{\omega}_S, \vec{\omega}_D)$ for all motor controllers. It provides an interface for higher level components, for instance, a user interfaces such as a joystick (a) in Fig. 3), the navigation module (b) in Fig. 3) which closes the position loop or the arm-control module (c) in Fig. 3) sending velocity requests to the platform. Therefore, the velocity control loop has to:

- 1) ensure adherence to the non-holonomic constraints
 - a) identify the valid configuration $(\vec{\varphi}_S, \vec{\omega}_D)$ and
 - b) derive a valid trajectory $(\vec{\varphi}_S, \vec{\omega}_S, \vec{\omega}_D, \vec{\omega}_D)$
 - c) respect the actuator limits $(\vec{\omega}_{S,u}, \vec{\omega}_{D,u})$
- 2) approach the commanded velocities fast
- 3) compensate the steer/drive-coupling $(\vec{\omega}_S, \vec{\omega}_D)$

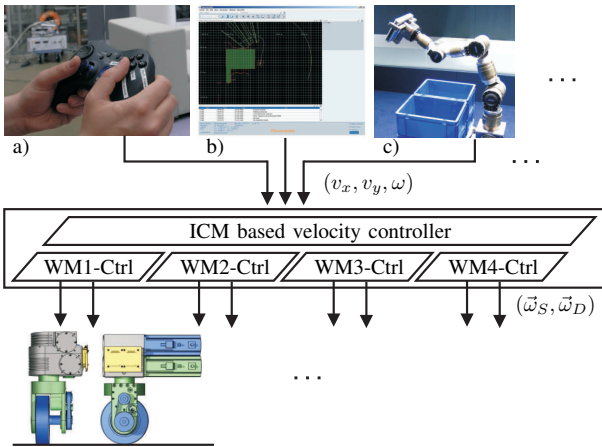


Fig. 3. Schematic of Care-O-bot 3's software-structure. The ICM based velocity controller synchronizes the motion of all wheels. The WM_X-Controllers synchronize the steer and drive motors of the single wheel modules.

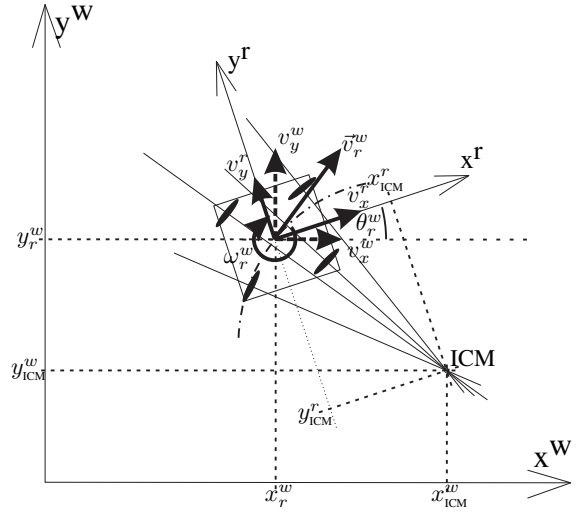


Fig. 4. Applied coordinate systems and ICM

III. ICM SPACE AND SINGULARITIES

A. Classical Definition

There are several corresponding definitions for the Instantaneous Centre of Motion (ICM). Within this work, the ICM is defined as the point in the world coordinate frame, which instantaneously does not change with respect to the robot when the latter moving. In Cartesian coordinates, it is represented as

$$\vec{x}_{ICM}^w = \begin{pmatrix} x_{ICM}^w \\ y_{ICM}^w \end{pmatrix} = \begin{pmatrix} x_r^w - v_{r,y}^w / \omega_r^w \\ y_r^w + v_{r,x}^w / \omega_r^w \end{pmatrix}, \quad (1)$$

where x_r^w, y_r^w and θ_r^w are components of the robot's position and orientation vector \vec{x}_r^w and $v_{r,x}^w, v_{r,y}^w, \omega_r^w$ are the components of the robot's twist \vec{t}_r^w

$$\vec{x}_r^w = \begin{pmatrix} x_r^w \\ y_r^w \\ \theta_r^w \end{pmatrix}, \quad \vec{t}_r^w = \begin{pmatrix} v_{r,x}^w \\ v_{r,y}^w \\ \omega_r^w \end{pmatrix}$$

in the world frame (Fig. 4). Transformation to the robot coordinate frame delivers

$$\vec{x}_{ICM}^r = \begin{pmatrix} x_{ICM}^r \\ y_{ICM}^r \end{pmatrix} = \begin{pmatrix} -v_{r,y}^r / \omega_r^r \\ +v_{r,x}^r / \omega_r^r \end{pmatrix} \quad (2)$$

for the ICM position, where $v_{r,x}^r, v_{r,y}^r$ and ω_r^r are the components of the robot's twist \vec{t}_r^r w.r.t the world frame

$$\vec{t}_r^r = \begin{pmatrix} v_{r,x}^r \\ v_{r,y}^r \\ \omega_r^r \end{pmatrix} = \begin{pmatrix} v_{r,x}^w \cos(\theta_r^w) + v_{r,y}^w \sin(\theta_r^w) \\ -v_{r,x}^w \sin(\theta_r^w) + v_{r,y}^w \cos(\theta_r^w) \\ \omega_r^w \end{pmatrix}$$

expressed in the robot coordinate frame. As we are not interested in the global behavior of the robot we confine our considerations on the robot-coordinate frame. For a more convenient writing the indicators of the coordinate system are omitted. \vec{t}_r^r is written instead of \vec{t}_r^w and \vec{x}_{ICM}^r instead of \vec{x}_{ICM}^w respectively.

B. Numerical Issues

The numerical problems arising while using an ICM-based representation of the twist \vec{t} are twofold. The first problem is that the transformation $f_{\text{ICM}}(\vec{t}_r)$ from the vector representation of the twist \vec{t}_r into the ICM representation (1),(2) is not injective. Information is lost and the ICM cannot be transformed back into the twist directly. The second, more severe problem, is the singularity arising when ω_r becomes zero, leading to unbounded growth of the controlled variables.

C. Alternative ICM Representations

These problems have been shown to be reduced if the ICM is expressed in a form similar to spherical coordinates [13]. The respective transformation equations are

$$\rho_{\text{ICM}} := \sqrt{v_{r,x}^2 + v_{r,y}^2 + (\omega_r \cdot d_{max})^2} \quad (3)$$

$$\varphi_{\text{ICM}} := \arctan_2 \left(\frac{v_{r,y}}{v_{r,x}} \right) \quad (4)$$

$$\theta_{\text{ICM}} := \arctan \left(\frac{\omega_r \cdot d_{max}}{\sqrt{v_{r,x}^2 + v_{r,y}^2}} \right) \quad (5)$$

for transforming the twist into the ICM representation. Where the constant factor d_{max} renders ω_r the same dimension as the linear velocities. The backwards transformation is

$$v_{r,x} = \rho_{\text{ICM}} \cdot \cos(\theta_{\text{ICM}}) \cdot \cos(\varphi_{\text{ICM}}) \quad (6)$$

$$v_{r,y} = \rho_{\text{ICM}} \cdot \cos(\theta_{\text{ICM}}) \cdot \sin(\varphi_{\text{ICM}}) \quad (7)$$

$$\omega_r = \frac{\rho_{\text{ICM}}}{d_{max}} \cdot \sin(\theta_{\text{ICM}}) \quad (8)$$

to transform back from the ICM representation into the twist \vec{t}_r . The evolution of the system configuration is fully described by the evolution of $(\rho_{\text{ICM}}, \varphi_{\text{ICM}}, \theta_{\text{ICM}})$:

$$\vec{\varphi}_S = \vec{f}_{\vec{k}_1, \vec{k}_2}(\varphi_{\text{ICM}}, \theta_{\text{ICM}}) \quad (9)$$

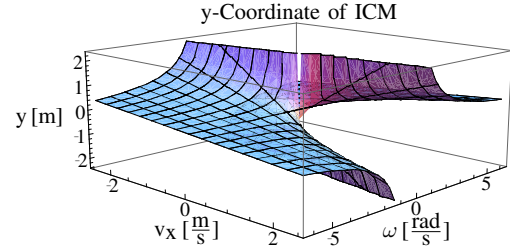
$$\vec{\omega}_S = J_{\vec{f}}(\varphi_{\text{ICM}}, \theta_{\text{ICM}}) \cdot \begin{pmatrix} \dot{\varphi}_{\text{ICM}} \\ \dot{\theta}_{\text{ICM}} \end{pmatrix} \quad (10)$$

$$\vec{\omega}_D = \vec{g}_{\vec{k}_1, \vec{k}_2}(\rho_{\text{ICM}}, \varphi_{\text{ICM}}, \theta_{\text{ICM}}) \quad (11)$$

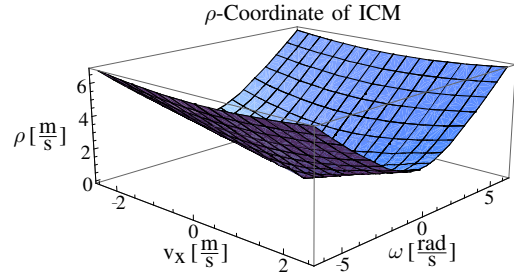
$$\dot{\vec{\omega}}_D = J_{\vec{g}}(\rho_{\text{ICM}}, \varphi_{\text{ICM}}, \theta_{\text{ICM}}) \cdot \begin{pmatrix} \dot{\rho}_{\text{ICM}} \\ \dot{\varphi}_{\text{ICM}} \\ \dot{\theta}_{\text{ICM}} \end{pmatrix}, \quad (12)$$

where (\vec{k}_1, \vec{k}_2) characterize the wheel orientations after startup. It has to be noted that for pure rotational motion equation (4) is not defined nor can φ_{ICM} be calculated by inverting equation (9). In this situation φ_{ICM} is neither observable nor controllable. However, the associated robot configuration $(\vec{\varphi}_S, \vec{\omega}_D)$ and the robot's rotational rate ω_r are still observable and controllable by $(\rho_{\text{ICM}}, \theta_{\text{ICM}})$ and equations (8 - 12).

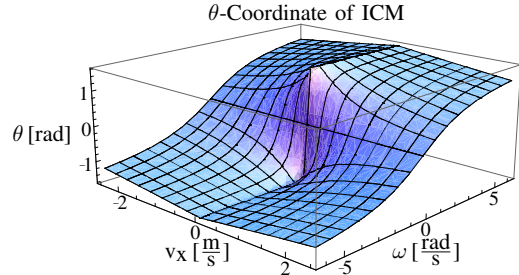
Figures 5 show the critical regions in the ICM representation. Figure 5(a) depicts the singularity arising in the y -component of the ICM if ω_r tends towards zeros. Figures 5(b) to 5(d) depict the critical regions for the components of the spherical ICM.



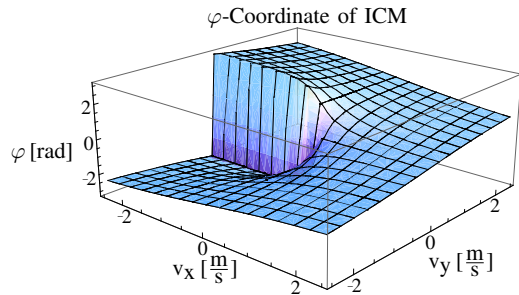
(a) Region around Singularity in y -coordinate of ICM



(b) Same region in (v_x, ω) -plane for ρ -parameter



(c) θ -parameter: not defined if $(v_x, v_y, \omega)^T = \vec{0}$



(d) φ -parameter: not defined for $(v_x, v_y)^T = \vec{0}$

Fig. 5. Visualization of the critical regions for transformation from velocity to cartesian and spherical ICM space (For Fig. 5(a) - 5(c) $v_y \equiv 0$)

IV. SINGULAR CONFIGURATIONS

In the case of a wheeled mobile robot with orientable standard wheels, the system degrades if the ICM $(x_{\text{ICM}}, y_{\text{ICM}})^T$ (2) comes near one of the wheel axis $(x_{a,i}, y_{a,i})^T$, $(d_{a,i}, \phi_{a,i})$ (Fig. 2) or

$$\begin{pmatrix} \varphi_{a,i} \\ \theta_{a,i} \end{pmatrix}_{1,2} = \begin{cases} \begin{pmatrix} \phi_{a,i} - \frac{\pi}{2} \\ \arctan\left(\frac{d_{m a x}}{d_{a,i}}\right) \end{pmatrix}, \\ \begin{pmatrix} \phi_{a,i} + \frac{\pi}{2} \\ -\arctan\left(\frac{d_{m a x}}{d_{a,i}}\right) \end{pmatrix} \end{cases} \quad (13)$$

respectively, when expressed in the spherical representation. For an arbitrary trajectory of the ICM in the (φ, θ) -plane $(\varphi_{\text{ICM}}, \theta_{\text{ICM}}, \dot{\varphi}_{\text{ICM}}, \dot{\theta}_{\text{ICM}})$, which passes close to but not through the steering axis of the i th wheel, the necessary steering rate of the wheel $\omega_{S,i}$ grows unbounded as the ICM approaches the steering axis.

A. Singularities and Actuator Limits

For a given change of the ICM in the cartesian space $(\dot{x}_{\text{ICM}}, \dot{y}_{\text{ICM}})^T$ the necessary steering velocity of the wheels $\vec{\omega}_S$ depending on the current ICM-position is calculated as follows:

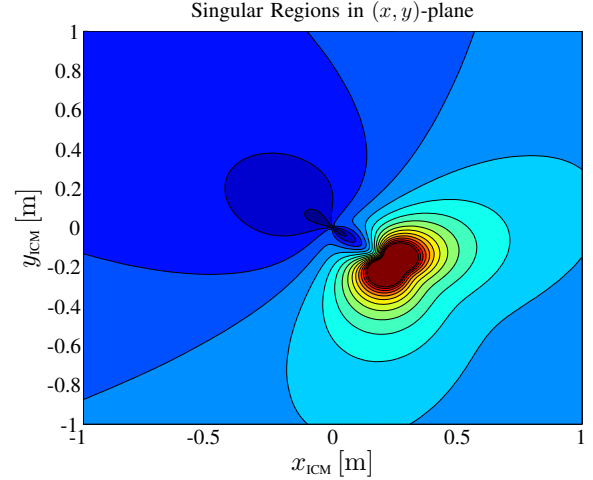
$$\begin{aligned} \omega_{S,i} &= \frac{\sqrt{\dot{x}_{\text{ICM}}^2 + \dot{y}_{\text{ICM}}^2} \cdot \sin(\phi_{\vec{x}_{\text{ICM}}} - \phi_{\vec{x}_{\text{ICM}}})}{\sqrt{\delta x_{\text{ICM},i}^2 + \delta y_{\text{ICM},i}^2}} \quad (14) \\ \phi_{\vec{x}_{\text{ICM}}} &= \arctan_2(\dot{y}_{\text{ICM}}, \dot{x}_{\text{ICM}}) \\ \phi_{\vec{x}_{\text{ICM}}} &= \arctan_2(\delta x_{\text{ICM},i}, \delta y_{\text{ICM},i}) \\ \begin{pmatrix} \delta x_{\text{ICM},i} \\ \delta y_{\text{ICM},i} \end{pmatrix} &= \begin{pmatrix} x_{\text{ICM}} - x_{a,i} \\ y_{\text{ICM}} - y_{a,i} \end{pmatrix} \end{aligned}$$

Thus, for a given maximum steering rate $\omega_{S,\text{max}}$ and a given change of the ICM $\dot{\vec{x}}_{\text{ICM}}$, a δ_{min} exists, with

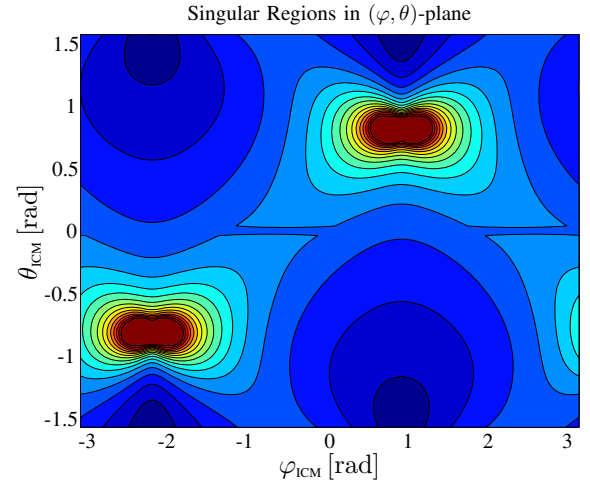
$$\left\{ \vec{x}_{\text{ICM}} \in \mathbb{R}^2 \mid \left| \vec{\delta}_{\text{ICM},i} \right| > \delta_{\text{min}} \right\} \rightarrow \omega_{S,i} < \omega_{S,\text{max}} \quad (15)$$

Vice versa, the critical ICM-positions \vec{x}_{ICM} for which (15) does not hold form a closed circular region around the i th wheel. According to (13) this critical region transforms into a closed and convex region in the spherical ICM space, as long as $\delta_{\text{min}} < d_{a,i}$. Thus, the singularities of the system can be represented within this ICM space by formulating a constant repulsive potential.

A worst case approximation of the necessary steering velocity for the ICM moving in the vicinity of the robot is depicted in figure 6. The calculations were performed for a constant absolute change $\left| (\dot{\varphi}_{\text{ICM}}, \dot{\theta}_{\text{ICM}})^T \right|$ of 1.5π rad/s for the ICM in its spherical representation. The direction of the ICM motion was resolved in steps of $\pi/50$ rad in the interval $[-\pi, +\pi]$. Figure 6(a) depicts a chart of the resulting maximum steering velocity for a single wheel with the steering axis at $x_a = 0.235$ m and $y_a = 0.185$ m in the robot coordinate frame. The according results for the velocity space in spherical coordinates are depicted in Figure 6(b).



(a) Steering velocities with respect to Position of ICM in cart. space



(b) Steering velocities with respect to Position of ICM in spher. space

Fig. 6. Worst case approximation for necessary steering velocity for an ICM motion with constant absolute speed of 1.5π rad/s. Dark red spaces indicate regions where the necessary steering velocity grows bigger than 8π rad/s, which is the maximum allowed steering rate for a wheel-module.

B. Modeling of the Potential Field

If the necessary steering velocities in the uncritical regions are neglected, the remaining problematic spots have a roughly convex form which can be approximated by an ellipsoidal shape. Due to this property we represent them as repulsive potentials in the well known form

$$U_{Si} = \begin{cases} \frac{1}{2}\eta \left(\frac{1}{r_{IS}} - \frac{1}{r_0} \right)^2 & \forall r_{IS} \leq r_0 \\ 0 & \forall r_{IS} \geq r_0 \end{cases} \quad (16)$$

introduced by Khatib [14], where r_0 and η allow to adapt size and incline of the potential. To adjust the shape of the repulsive potentials to the form of the critical regions, r_{IS} was chosen to be an ellipsoidal distance function

$$r_{IS}^2 = \frac{(\varphi_{\text{ICM}} - \varphi_{a,i})^2}{a^2} + \frac{(\theta_{\text{ICM}} - \theta_{a,i})^2}{b^2} \quad (17)$$

with the parameters a and b defining the principal axis of the ellipse. The resulting force imposed from a singularity

on the ICM is:

$$F_{Si} = \begin{cases} \eta \left(\frac{1}{r_{IS}} - \frac{1}{r_0} \right) \frac{1}{r_{IS}^2} \frac{\partial r_{IS}}{\partial \vec{x}_{ICM}} & \forall r_{IS} \leq r_0 \\ 0 & \forall r_{IS} \geq r_0 \end{cases} \quad (18)$$

Analogously, the attracting force is calculated to

$$F_T = -k_\nu (\dot{\vec{x}}_{ICM} - \nu \dot{\vec{x}}_{ICM,d}), \quad (19)$$

where $\dot{\vec{x}}_{ICM}$ is the current first derivative of the ICM in the (φ, θ) -plane, $\dot{\vec{x}}_{ICM,d}$ is the value, the first derivative of the ICM would take, if only attracting and frictional forces were considered

$$\dot{\vec{x}}_{ICM,d} = \frac{k_p}{k_\nu} (x_{ICM,d} - x_{ICM}), \quad (20)$$

k_p is the proportionality factor between control deviation and force, k_ν is the friction coefficient which stabilizes the controller and ν

$$\nu = \min \left(1, \frac{v_{max}}{|\dot{\vec{x}}_{ICM,d}|} \right) \quad (21)$$

ensures that the velocity does not exceed a certain limit. The variable ρ_{ICM} - representing the total velocity of the robot - is controlled independently from the φ_{ICM} and θ_{ICM} variables - representing the kinematic configuration of the robot.

The potential field resulting when this controller is particularized for Care-O-bot 3's specific kinematics is visualized in Figure 7. The attractive potential was generated for a target configuration set to $(\varphi, \theta) = (\frac{1}{2}\pi \text{ rad}, \frac{2}{7}\pi \text{ rad})$. Figure 7(a) depicts the resulting potential in the cartesian plane and Figure 7(b) shows it in the (φ, θ) -plane respectively.

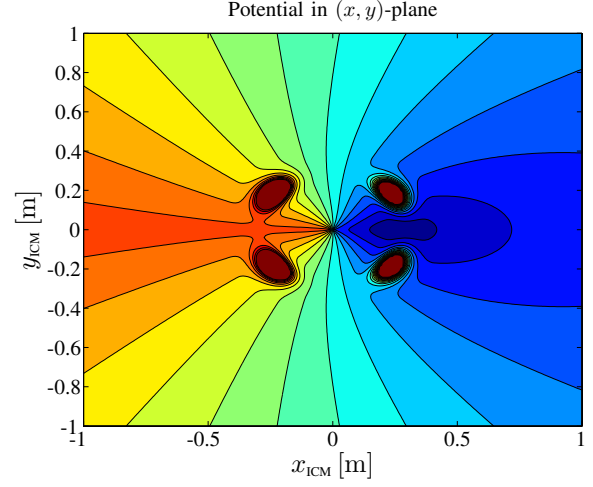
V. RESULTS

The discussed control structure was tested simulatively in a Matlab Simulink environment and experimentally on the mobile platform of Care-O-bot 3 (Sec. II).

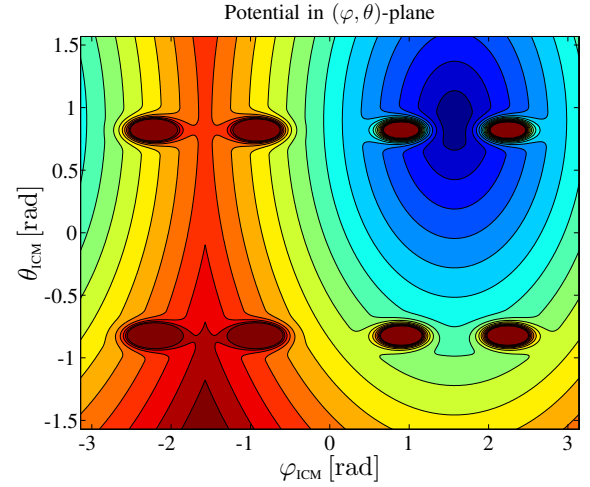
A. Simulation Results

The system is simulated in continuous time, while the controller is run in discrete time with a fixed step size of 50 ms. The simulation takes into account a communication delay between controlled system and controller of 10 ms and restrictions on rotational rate and possible acceleration of the wheel modules.

Figures 8 show the result for an arbitrary sequence over a simulation period of 10 s. The system's starting configuration was set to $(\rho, \varphi, \theta) = (0, 0, 0)$ (configuration for straight forward motion). At time $t = 1$ s the target configuration changes to $(\rho, \varphi, \theta) = (1, 0, 0.8)$ (forward driven left turn). Then, it is set to $(1, 3, 1.23)$ (tight left turn superposed with diagonal - left front corner - drive) at $t = 2.6$ s and to $(1, 0, -1.4)$ (tight right turn - close to rotation on the spot; $t = 5.3$ s), before at the end ($t = 9$ s) ρ is set to 0 again. Figure 8(a) shows the resulting path of the ICM in the (φ, θ) -plane. The according set point values for (ρ, φ, θ) are plotted in figure 8(b) together with the controlled values. Figure 8(c) shows control error, resulting forces and velocity for (φ, θ) .



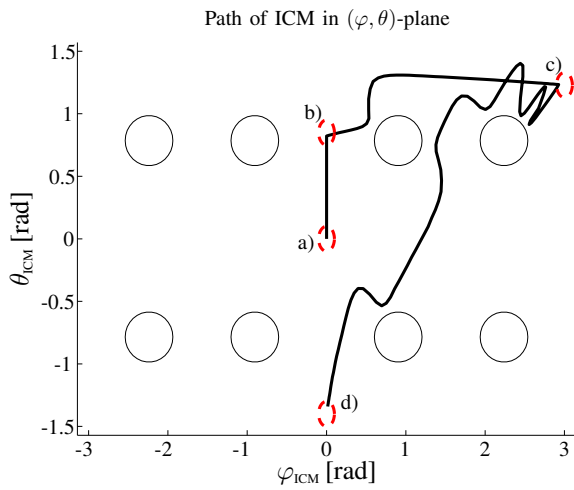
(a) Resulting potential field (repulsive and attractive) in Cartesian space



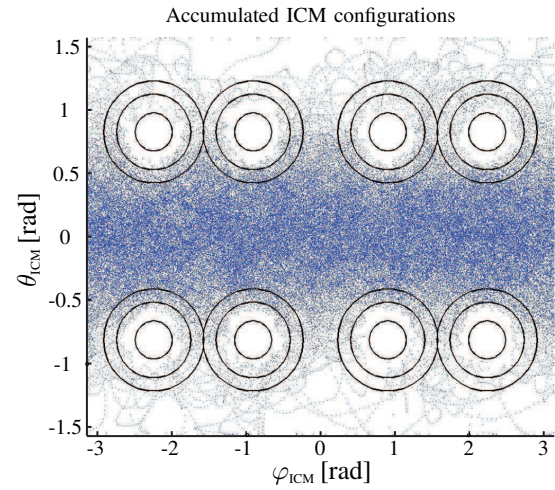
(b) Resulting potential field (repulsive and attractive) in spherical space

Fig. 7. Potential field of the controller for (φ, θ) resulting from repulsive potentials of all wheels and the attractive potential for a goal configuration at $(\varphi, \theta) = (\frac{1}{2}\pi \text{ rad}, \frac{2}{7}\pi \text{ rad})$, with $k_p = 6$, $\eta = 8$, $r_0 = 1.4$, $a = 0.5$, $b = 0.15$. (dark blue: low potential; dark red: high potential)

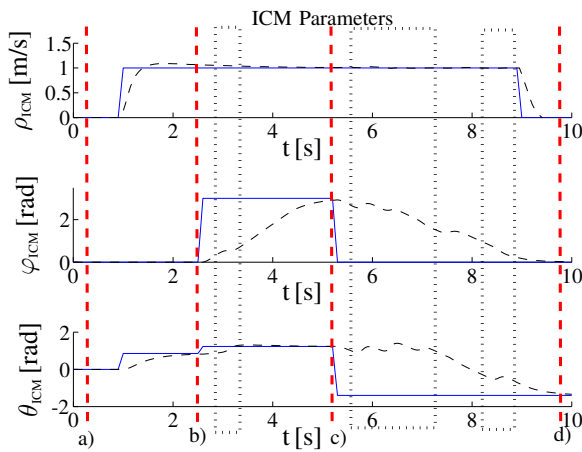
In figure 8(a) one can see how the repulsive potentials redirect the ICM away from the singular configurations and towards the goal. A critical situation is encountered at start of the third section (from target c) to d)), where the optimal path runs almost through the middle of the singular region. This is problematic for two reasons. First, such situations create saddlepoints, in which the gradient and thus the resulting force becomes zero. However, such configurations are unstable and thus in practice, due to disturbances, it is unlikely to get stuck. Second, as calculations of the controller are performed in discrete time-steps the system might dive too deep into the repulsive potential, before recalculating the force. This can cause oscillations with increasing amplitude in such regions (Fig. 8(a)). One can address this problem for instance by slowing down the controller or reducing the time-steps which reduces the maximum change of the ICM configuration between two control cycles and thus the possible intrusion into a repulsive potential. A possibility



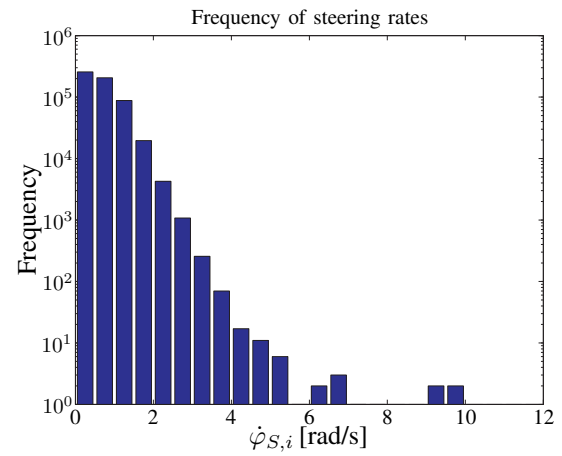
(a) Resulting path of ICM in the (φ, θ) -plane



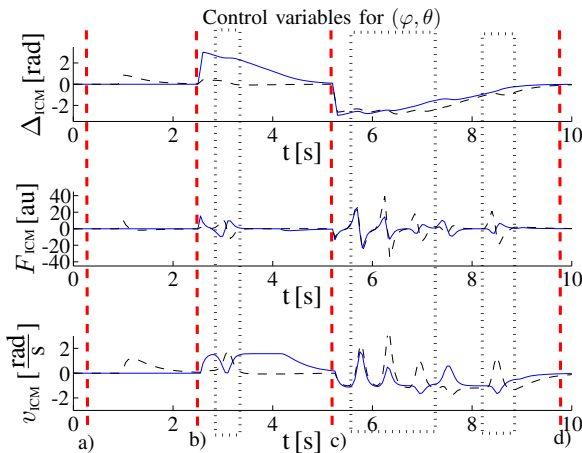
(a) Accumulated ICM configurations in the (φ, θ) -plane



(b) Set point values (blue solid) and resulting controlled values (black dashed) for (ρ, φ, θ)



(b) Histogram of corresponding Steering velocities for all wheels



(c) Control error, resulting force and commanded velocity for φ (red dotted) and θ (green dash-dotted)

Fig. 8. Results for an arbitrary path of the ICM in the (φ, θ) -plane for a sequence of three arbitrary target configurations(a) $(\varphi, \theta) = (0, 0)$; b) $(\varphi, \theta) = (0, 0.8)$; c) $(\varphi, \theta) = (3, 1.23)$; d) $(\varphi, \theta) = (0, -1.4)$). The Target configurations are indicated with red dashed lines. The black dotted rectangles (Fig. 8(b) and Fig. 8(c)) indicate situations where the ICM was under the influence of the repulsive potentials.

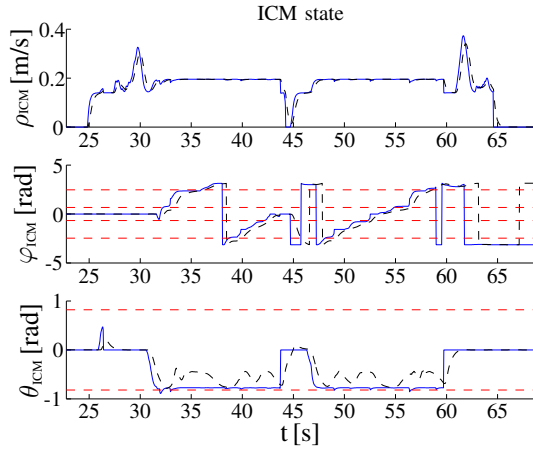
Fig. 9. ICM configurations (blue dots) accumulated during a simulated 2 hour run. Set point values were randomly generated every 0.5 s. Controller was run at 20 Hz. Black circles mark influence region of repulsive potentials.

on cost of the computational complexity, is to predict the next ICM configuration and adapt the current force command (e.g. on behalf of additional interpolation steps), if the next configuration would dive deeply into the repulsive potential.

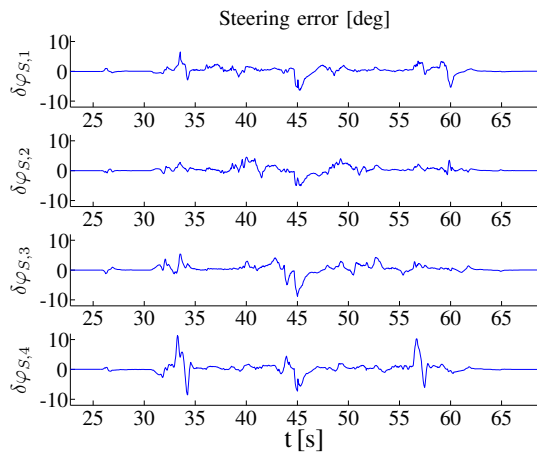
Figure 9 depicts results obtained during a 2 hour simulation run. During this simulation target configurations were generated randomly every 0.5 s on the whole (φ, θ) -plane. Figure 9(a) depicts the accumulated resulting states the system took during the 2 hour run. the histogram (Fig. 9(b)) shows the frequency of the commands generated for the steering motion of the wheels. As one can see the ICM did avoid the proximity of the singular regions and the commanded steering rates all stayed significantly lower as the maximum of 24 rad/s.

B. Experimental results

During the experiments the robot is controlled remotely via a Joypad, generating the velocity commands. Figures 10 depict the results for a 40 s run in which the system was repeatedly driven close to singular configurations. In fig-



(a) Set point values (blue solid) and resulting controlled values (black dashed) for (ρ, φ, θ)



(b) Error in steering angle for all wheels

Fig. 10. Experimental results obtained with Care-O-bot 3 during a 40s testdrive where the robot was controlled remotely. The red dashed lines indicate the critical values for φ_{ICM} and θ_{ICM} , on which the singular spots are situated.

ure 10(a) one can see how the system follows the target configuration and how it is repelled if this configuration passes close to a singularity. As shown in Figure 10(b) the errors in the wheel's steering angles $\delta\varphi_S$ stay reasonably small during these maneuvers.

VI. CONCLUSIONS AND FUTURE WORKS

Within this work the problem of singularities arising from wheeled mobile robots with orientable standard wheels is addressed. The arising singularities are classified into ones, which are dependent from the mathematical representation of the system and ones which are directly related to the system's kinematic configuration. A strategy to mitigate the influence of the first type was revised and a potential field based approach to address the second type is proposed. Simulation and experimental results support the validity of this method.

Current work focuses on an adaption of system representation and potential field formulation to exploit the redundancy of the systems configuration space as well as to reduce the problems related to the finite time steps.

VII. ACKNOWLEDGMENTS

This work was partially funded within the EU Project COGNIRON ("The Cognitive Robot Companion" - www.cogniron.org) under Contract FP6-IST-FET-002020.

Additional funding was granted within the research project DESIRE by the German Federal Ministry of Education and Research (BMBF) under grant no. 01IME01A

REFERENCES

- [1] B. Graf, M. Hans, R.D. Schraft, "Care-O-bot II - Development of a Next Generation Robotic Home Assistant", *Autonomous Robots*, Vol. 16, Issue 2, March 2004, pp.193-205
- [2] R. Siegwart and I.R. Nourbakhsh, "Introduction to Autonomous Mobile Robots", *Intelligent Robotics and Autonomous Agents series*, MIT Press, Cambridge Massachusetts, 2004
- [3] P. Muir, C. Neuman, "Kinematic Modeling for Feedback control of an Omnidirectional Wheeled Mobile Robot", *IEEE International Conference on Robotics and Automation*, 1987, pp. 1772-1778
- [4] K. Tadakuma, R. Tadakuma, "Mechanical Design of "Omni-Ball": Spherical wheel for Holonomic Motion", *IEEE Conference on Automation Science and Engineering*, Scottsdale, Sept. 2007, pp.788-794
- [5] G. Campion, G.Bastin and B. D'Andréa-Novel, "Structural Properties and Classification of Kinematic and Dynamic Models of Wheeled Mobile Robots", *IEEE Transactions on Robotics and Automation*, Vol. 12, No. 1, Feb. 1996, pp 47-62
- [6] T. Burke and H.F. Durrant-Whyte, "Kinematics for Modular Wheeled Mobile Robots", *IEEE/RSJ International Conference on Intelligent Robots and Systems*, Yokohama, Jul. 1993, pp 1279-1286
- [7] K.L. Moore and N.S. Flann, "A Six-Wheeled Omnidirectional Autonomous Mobile Robot", *IEEE Control Systems Magazine*, Vol. 20, Issue 6, Dec. 2000, pp 53-66
- [8] Y. Mori, E. Nakano, T. Takahashi, "Mechanism, Control and Design Methodology of the Nonholonomic Quasi-Omnidirectional Vehicle ODV9", *The International Journal of Robotics Research*, Vol. 21, No. 5-6, May-June 2002, pp 511-525
- [9] D.B. Reister and M.A. Unseren, "Position and Constraint Force Control of a Vehicle with Two or More steerable Drive Wheels", *IEEE Transactions on Robotics and Automation*, Vol. 9, No. 6, Dec. 1993, pp 723-731
- [10] M. Hashimoto, N. Suizu, I. Fujiwara and F. Oba, "Path tracking Control of a Non-Holonomic Modular Omnidirectional Vehicle", *IEEE International Conference on Systems, Man and Cybernetics*, Vol. 6, Tokyo, Oct. 1999, pp 637-642
- [11] M. Lauria, I. Nadeau, P. Lepage, Y. Morin, P. Giguère, F. Gagnon, D. Létourneau and F. Michaud, "Design and Control of a Four Steered Wheeled Mobile Robot", *IEEE 32nd Annual Conference on Industrial Electronics*, Nov. 2006, pp 4020-4025
- [12] B. Thuilot, B. D'Andréa-Novel and A. Micaelli, "Modeling and Feedback Control of Mobile Robots Equipped with Several Steering Wheels", *IEEE Transactions on Robotics and Automation*, Vol. 12, No. 3, June. 1996, pp 375-390
- [13] C.P. Connette, A. Pott, M. Hägele, A. Verl, "Control of an Pseudo-Omnidirectional, Non-holonomic, Mobile Robot based on an ICM Representation in Spherical Coordinates", accepted to *IEEE Conference on Decision and Control*, Cancun, 9-11 December 2008
- [14] O. Khatib, "Real-Time Obstacle Avoidance for Manipulators and Mobile Robots", *The International Journal of Robotics Research*, Vol. 5, No. 1, Spring 1986, pp 90-98
- [15] B. Krogh, "A Generalized Potential Field Approach to Obstacle Avoidance Control", *SME Conference on Robotics Research: The Next Five Years and Beyond*, Bethlehem Pennsylvania, August 1984
- [16] E. Rimon, D.E. Koditschek, "Exact Robot Navigation Using Artificial Potential Functions", *IEEE Transactions on Robotics and Automation*, Vol. 8, No.5, October 1992, pp 501-518
- [17] L. Chengqing, M.H. Ang Jr, H. Krishnan, L.S. Yong, "Virtual Obstacle Concept for Local-minimum-recovery in Potential-field Based Navigation", *IEEE International Conference on Robotics and Automation*, San Francisco, April 2000, pp 983-988
- [18] S. Shimoda, Y. Kuroda, K. Iagnemma, "Potential Field Navigation of High Speed Unmanned Ground Vehicles on Uneven Terrain", *IEEE International Conference on Robotics and Automation*, Barcelona, April 2005, pp 2839-2844